Available online at www.sciencedirect.com
SCIENCE DIRECT®
Finite Elements in Analysis and Design 40 (2004) 1619–1640
FINITE ELEMENTS IN ANALYSIS AND DESIGN
www.elsevier.com/locate/finel

Two scale response and damage modeling of composite materials

P. Raghavan, S. Li, S. Ghosh*

Department of Mechanical Engineering, The Ohio State University, Columbus, OH, USA

Received 27 October 2003; accepted 30 November 2003

Abstract

This paper presents an adaptive multi-level computational model that combines a conventional displacement-based finite element model with a microstructural Voronoi cell FEM (VCFEM) for multi-scale analysis of composite structures with non-uniform microstructural heterogeneities as obtained from optical or scanning electron micrographs. Three levels of hierarchy, with different resolutions, are introduced to overcome shortcomings posed by modeling and discretization errors. These are: (a) level-0 of pure macroscopic analysis; (b) level-1 of macro–micro coupled modeling for implementing switching criteria from macroscopic analyses to pure microscopic analyses; and (c) level-2 regions of pure microscopic modeling. An example of a double lap aluminum composite bonded joint with perfect interface is solved to demonstrate the ability of the multi-scale computational model in analyzing complex heterogeneous structures. For damaging materials, a continuum damage mechanics (CDM) model is developed for fiber-reinforced composites with interfacial debonding. The model is constructed from and calibrated with rigorous micromechanical analysis of the representative volume element using the VCFEM that is followed by homogenizing microscopic variables using asymptotic homogenization. The CDM results are compared with those obtained by homogenization of micromechanical analysis and the range of validity of homogenized solutions is identified.

Keywords: Composite materials; Homogenization; Multi-scale modeling; Voronoi cell FEM; Continuum damage mechanics

1. Introduction

Heterogeneous structures are conventionally analyzed with properties obtained from homogenization [1] of response at smaller (meso-, micro-) length scales. Analysis of composite materials is often

* Corresponding author. Department of Aerospace Engineering, Applied Mechanics & Aviation, Ohio State University, 209 Boyd Laboratory, 155 West Woodruff Avenue, Columbus, OH 43210-1181, USA. Tel.: +1-614-292-2599; fax: +1-614-292-7369.
E-mail address: ghosh.5@osu.edu (S. Ghosh).

0168-874X/$ - see front matter © 2003 Elsevier B.V. All rights reserved.
doi:10.1016/j.finel.2003.11.003

performed by the method of homogenization wherein the macroscopic properties are obtained by averaging stresses and strains over a periodic representative volume element (RVE). The application of homogenization methods suffer from some shortcomings with respect to limitations in the assumptions of macroscopic uniformity and RVE periodicity. The uniformity assumption is not appropriate in critical regions of high gradients like free edges [2], interfaces, material discontinuities and most importantly in regions of evolving damage. Periodicity of simple unit cells is also unrealistic for non-uniform microstructures, particularly in the presence of clustering. Even with uniform distribution of microstructures, evolving localized stresses or strains can violate the periodic assumptions. Problems like this have been tackled effectively by global-local techniques [3–5]. Sub-structuring in these multiple-scale analysis methods differentiate between regions requiring different resolutions, and enable global analysis in some parts of the domain and zoom in for complete microscopic modeling at regions of high gradients.

Multiple-scale analysis using adaptive multi-level modeling with the microstructural Voronoi cell FEM (VCFEM) model has been conducted by Ghosh et al. [4,6] for modeling problems with evolving damage and for free-edge problems in composites. Adaptivity, for controlling discretization error and the modeling error, is a desirable feature in multiple-scale modeling for selecting appropriate regions of enrichment to minimize discretization and modeling errors.

In the present work, the adaptive multi-level method is advanced to comprehensively address issues of both discretization and physically based modeling error. The method is applied to linear elastic composite microstructure and a non-linear problem with evolving fiber/matrix interfacial damage. The hierarchical model consists of three essential levels in this work, (i) purely macroscopic domain (level-0) with homogenized material parameters; (ii) a macro–micro domain (level-1) with the micro-domain represented by the periodic repetition of a RVE and (iii) purely microscopic domain (level-2) where the RVE ceases to exist and extended microstructural regions with delineation of distributed heterogeneities need to be modeled. An intermediate layer is used between the macroscopic and microscopic regions for smooth transition. The level-1 domain is utilized to estimate criteria for switching from macroscopic to microscopic calculations from values of variables in the RVE. Physically based error indicators are developed for transitioning from macroscopic to microscopic domain computations. All microstructural computations of arbitrary heterogeneous domains are conducted using the adaptive Voronoi cell finite element model [7]. Statistical functions are used to assess the extent of the RVE domains for non-uniform microstructures. For the macroscopic domains, *h*- and *hp*- adaptation are executed using conventional error indicators based on the energy norm. The model is tested for a realistic problem with macroscopic stress risers.

A continuum damage model is developed for composite materials with non-uniform microstructures from detailed micromechanical analysis with damage. Interfacial debonding between matrix and inclusion phases of the microstructure is considered as the damage mode in this paper. Interfacial debonding is simulated using cohesive zone models. The micromechanical analyses in each RVE are conducted with the VCFEM [8], in which cohesive zone models are used to model interfacial debonding. The asymptotic homogenization method is used to evaluate macroscopic damage variables and their evolution laws. Based on the effectiveness of the anisotropic models, the strain based anisotropic damage model developed in [9] is modified for damage in anisotropic composite materials. Parameters which characterize anisotropic stiffness degradation are found to vary with evolution of microstructural state variables. Consequently, a set of macroscopic strain paths is chosen, along which anisotropic parameters are evaluated. Numerical examples are conducted for demonstrating the

effectiveness of the continuum damage mechanics (CDM) model in predicting damage in composite structures.

2. The adaptive multi-scale computational model

The adaptive multi-scale computational model developed in this paper has three main computational subdomains as shown in Fig. 1 and is discussed next.

2.1. Computational subdomain level-0

Level-0 subdomains encompass regions of macroscopic analysis using effective properties obtained by homogenization of RVE. This level is valid in regions where macroscopic gradients in variables like stresses or strains are relatively small. For each element in the level-0 subdomain, an RVE is identified and the asymptotic homogenization method is then used for obtaining effective material properties. A brief overview of the asymptotic homogenization method is provided next.

2.1.1. The asymptotic homogenization method

Boundary value problems in a heterogeneous domain Ω^ε are assumed to satisfy the equations of linear elasticity, given as

$$\begin{aligned} \text{Equilibrium} &: \sigma^\varepsilon_{ij,j} = -f_i, \\ \text{Kinematics} &: e^\varepsilon_{kl} = \frac{1}{2}\left(\frac{\partial u^\varepsilon_k}{\partial x^\varepsilon_l} + \frac{\partial u^\varepsilon_l}{\partial x^\varepsilon_k}\right), \\ \text{Constitutive relations} &: \sigma^\varepsilon_{ij} = E^\varepsilon_{ijkl} e^\varepsilon_{kl} \text{ in } \Omega^\varepsilon, \end{aligned} \tag{1}$$

where σ^ε_{ij}, e^ε_{ij} and u^ε_i are stress, strain and displacement fields, respectively. The scale parameter $\varepsilon = l_y/l_x$ (l_y, l_x correspond to length scales in the microscopic and macroscopic domains,

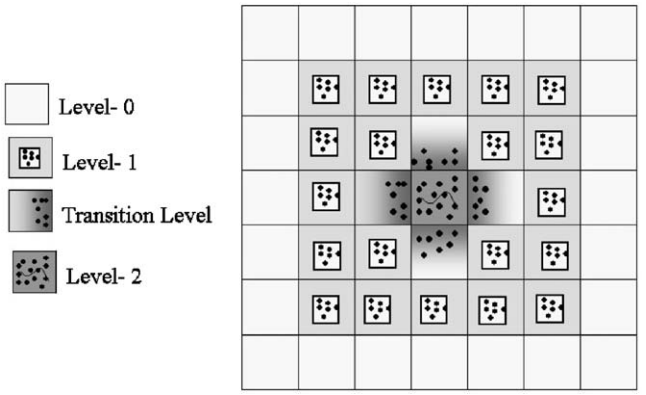

Fig. 1. Multi-level mesh showing different levels for the multi-scale model.

respectively) is typically an infinitesimally small number. Since computational analysis of this problem will be prohibitively expensive due to the presence of large number of heterogeneities, most analysts solve an equivalent homogenized version of the problem using macroscopic effective properties obtained by averaging microscopic variables. A powerful method that has been developed in conjunction with computational analysis of heterogeneous materials is the asymptotic expansion homogenization method [1,10]. In this method, the displacement field in a heterogeneous domain is expanded asymptotically about its values at a macroscopic point $\mathbf{x}$, in terms of the microscopic coordinates $\mathbf{y}$ as

$$u_i^{\varepsilon}(\mathbf{x}) = u_i^0(\mathbf{x},\mathbf{y}) + \varepsilon u_i^1(\mathbf{x},\mathbf{y}) + \varepsilon^2 u_i^2(\mathbf{x},\mathbf{y}) + \cdots, \quad \mathbf{y} = \frac{\mathbf{x}}{\varepsilon}. \tag{2}$$

Using Eq. (2) in kinematics, constitutive and equilibrium relations of Eqs. (1) and equating various powers of ε in conjunction with periodicity conditions, the volume average of microscopic stresses yielding the homogenized stiffness tensor E^{H}_{ijkl} can be obtained as

$$E^{\mathrm{H}}_{ijkl} = \langle \hat{\sigma}^{kl}_{ij} \rangle_Y = \frac{1}{|Y|} \int_Y \hat{\sigma}^{kl}_{ij}\, \mathrm{d}Y = \frac{1}{|Y|} \int_Y E^{\varepsilon}_{ijpm} \left(\delta_{kp}\delta_{lm} + \frac{\partial \chi^{kl}_p}{\partial y_m} \right) \mathrm{d}Y, \tag{3}$$

where $\hat{\sigma}^{kl}_{ij}$, χ^{kl}_p are the microscopic stresses and characteristic deformation modes, δ is the Kronecker delta and Y is the RVE domain. The macroscopic stress–strain relation then takes the form

$$\Sigma_{ij}(\mathbf{x}) = \left\langle E^{\varepsilon}_{ijkl} \left(\delta_{km}\delta_{ln} + \frac{\partial \chi^{mn}_k}{\partial y_l} \right) \frac{\partial u^0_m}{\partial x_n} \right\rangle_Y = E^{\mathrm{H}}_{ijmn} e_{mn}(\mathbf{x}), \tag{4}$$

where the homogenized variables are $\mathbf{\Sigma}(\mathbf{x}) = \langle \sigma^{\varepsilon}(\mathbf{x},\mathbf{y}) \rangle_Y$ and $\mathbf{e}(\mathbf{x}) = \langle e^{\varepsilon}(\mathbf{x},\mathbf{y}) \rangle_Y$. The components of the homogenized stiffness matrix E^{H}_{ijkl} are calculated by detailed solution of separate boundary value problems of the entire RVE. The loading in each of these problems is in the form of imposed unit macroscopic strains. For periodicity, nodes on the boundary which are separated by the periods Y_1, Y_2, Y_3 along one or more coordinate directions, the displacement constraints can be expressed as

$$u_i(x_1, x_2, x_3) = u_i(x_1 \pm k_1 Y_1, x_2 \pm k_2 Y_2, x_3 \pm k_3 Y_3), \quad i = 1,2,3, \tag{5}$$

where k_1, k_2, k_3 may assume the values 0 or 1, depending on the node locations.

2.2. Computational subdomain level-1

Level-1 subdomains are intended as 'transition' regions, where microscopic information in the RVE is used to decide whether extended microscopic computations are necessary for these regions. They are seeded in regions of locally increasing gradients of macroscopic variables in the pure level-0 simulations. These gradients may be caused by microscopic non-homogeneity in the form of large localized stresses and strains, or when the microstructure faces possible damage initiation or localization. Computations in this region are still based on assumptions of macroscopic uniformity and periodicity of the RVE. Concurrent with macroscopic simulations, computations are executed in the microstructure to monitor variables in the RVE. The computations in elements belonging to the level-1 domain undergo a sequence of finite element analyses as follows.

(a) Microstructural analysis of the RVE, subjected to the sequence of unit macroscopic strains or increments with periodicity boundary conditions to generate homogenized tangent modulus (E^{H}_{ijkl}).

(b) Macroscopic analysis of the structure using (E^{H}_{ijkl}) of step (a), to evaluate macroscopic variables e.g. stresses and strains due to applied loads.

(c) Microstructural analysis of the RVE at each sampling point (e.g. integration point) of macroscopic elements, with actual macroscopic strains and increments obtained from step (b) and periodicity conditions on the RVE boundary. Microscopic stresses and strains ($\sigma^{e}, \varepsilon^{e}$) are thus calculated in the RVEs of each element.

Macroscopic level-0/1 calculations are performed with conventional displacement based finite element method while all microscopic calculations in the RVE for level-1 elements are performed using VCFEM which is discussed in the following section.

2.3. Computational subdomain level-2

Level-2 regions are characterized as those with significant microstructural non-uniformities in the form of high local stresses or strains that would occur e.g. near a crack tip or free edge. High gradients in macroscopic variables and loss of RVE periodicity are expected in those regions. Scale effects are important in these regions, resulting in mesh-dependence of pure macroscopic computations. The high-resolution model for level-2 elements with many heterogeneities entails prohibitively large computations with conventional finite element models. Consequently, the microstructure based VCFEM, which has been developed in [7,8,11,12] for modeling non-uniform heterogeneous materials is used for analyzing the level-2 elements. Extensive microstructural regions, obtained from micrographs, are efficiently modeled by this approach. In VCFEM, the computational mesh consists of multi-sided Voronoi polygons that naturally evolve by tessellation of the microstructure. Each element in VCFEM consists of a heterogeneity (inclusion or void) with its immediate surrounding matrix. Accuracy of analysis is maintained for these relatively large multiphase elements by incorporating observed behavior of stress fields from micromechanics in an assumed stress hybrid finite element formulation [12]. VCFEM is estimated to be ~ 60–70 times lower than most commercial FEM packages for modeling complex microstructures.

3. Various features of the multi-level computational model

3.1. Estimating statistically equivalent RVEs for non-uniform microstructures

Macroscopic analysis of a composite structure, requires that an appropriate RVE be identified for each macroscopic point. RVEs can be readily identified for a regular arrangement of fibers like rectangular or hexagonal distributions. However, microstructures from real composite materials hardly possess regular distribution as shown in Fig. 2(b). In Fig. 2 an aluminum composite bonded joint and the corresponding microstructure from an optical micrograph near point A are shown. The fibers are assumed to be aligned perpendicular to the plane of paper. Since this microstructure distribution is random, an RVE can be obtained only in a statistical sense and attention is focused on identifying a statistically equivalent RVE (SERVE), which would exhibit a macroscopic behavior that is equivalent to the average behavior of the corresponding microstructure.

The microstructure shown in Fig. 2(b) corresponds to macroscopic point A only. Since the construction of SERVEs for the entire plate would require a large number of micrographs from various

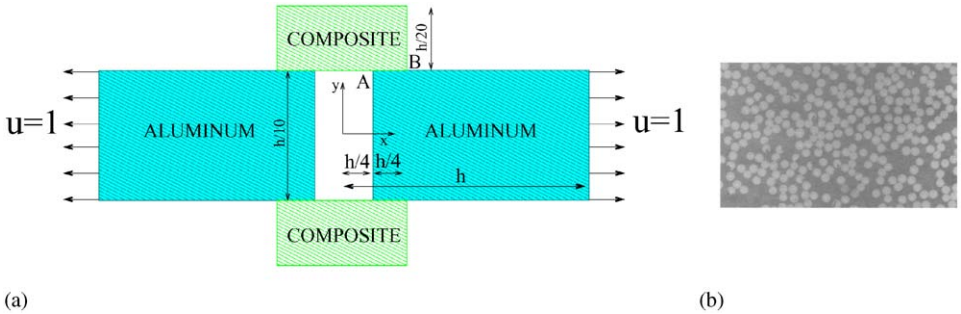

Fig. 2. (a) A double-lap aluminum/boron–epoxy composite bonded joint showing dimensions and loads; (b) Optical micrograph of the microstructure near point A.

representative points in the plate, an assumption is made that, this is a representative microstructure for the entire plate. The representative size of the SERVE is identified by the use of statistical functions, e.g. correlation functions. Pyrz [13] has introduced "marked correlation functions" for characterizing the length scales defined as the region of influence in a heterogeneous neighborhood on pre-disposed response fields like stresses and strains. The marked correlation function for a heterogeneous domain of area A containing N fibers may be expressed as

$$M(r) = \frac{\mathrm{d}H(r)/\mathrm{d}r}{g(r)}, \tag{6}$$

where $H(r) = \frac{1}{m^2}\frac{A}{N^2}\sum_i^N \sum_{k=1}^{k_i} m_i m_k(r)$. In the above equation, m_i is a mark associated with ith fiber, k_i is the number of fibers which have their centers within a circle of radius r around the ith fiber, m_k are the marks of those fibers and m is the mean of all the marks. Marks in the marked correlation function can be any field variable for example, the maximum principal stress, Von Mises stress etc. associated with each fiber. $H(r)$ is called the mark intensity function and $g(r)$ is the pair distribution function defined as

$$g(r) = \frac{1}{2\pi r}\frac{\mathrm{d}K(r)}{\mathrm{d}r}, \tag{7}$$

where $K(r)$ is a second order intensity function which is explained in [14]. While $K(r)$ can distinguish between different patterns, the pair distribution function $g(r)$ characterizes the intensity of inter fiber distances. From the definition it can be seen that the marked correlation function associates field variables with morphology of the microstructure. The radius of influence R_{inf} may be inferred from a plot of $M(r)$ vs. r, in which $M(r)$ stabilizes as r approaches R_{inf}. Plot of $M(r)$ vs. r for the microstructure loaded in simple tension and biaxial tension is shown in Fig. 3. From the value of R_{inf}, the RVE is found to contain 18 fibers. Convergence of macroscopic and microscopic stresses with increasing RVE sizes has been studied in detail in [15,16].

Upon determining the radius of influence R_{inf}, a method of constructing the SERVE boundary by repeating the group of fibers periodically is adopted in this work. The local microstructure is first constructed by repeating the randomly distributed fibers obtained from statistical analysis in both the y_1- and y_2-directions for several period lengths. Periodic repetitive fibers are placed at (y_1, y_2), $(y_1 \pm k_1 Y_1, y_2)$, $(y_1, y_2 \pm k_2 Y_2)$ and $(y_1 \pm k_1 Y_1, y_2 \pm k_2 Y_2)$, where k_1, k_2 are integers. The period lengths Y_1 and Y_2 are selected such that the volume fraction of the RVE matches with that

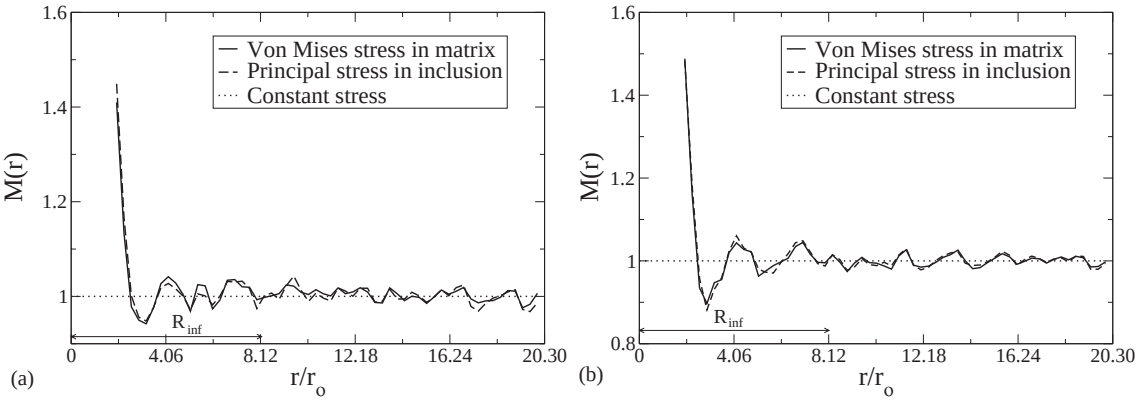

Fig. 3. Marked correlation functions $M(r)$ for (a) uniaxial loading and; (b) biaxial loading.

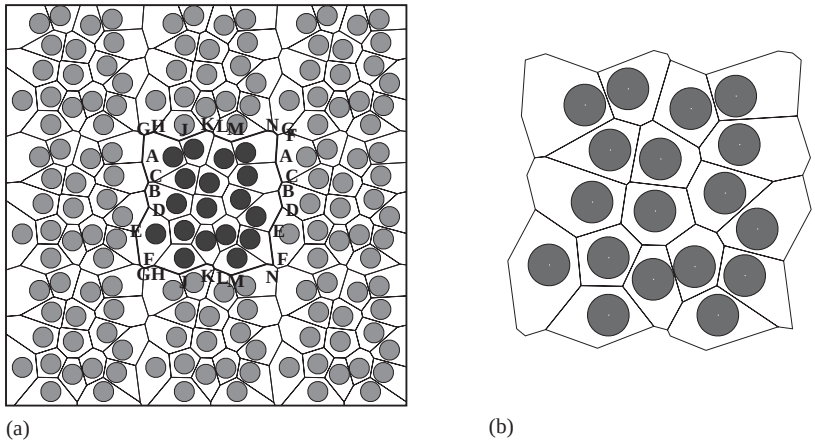

Fig. 4. (a) Construction of periodic RVE with non-straight edges; (b) SERVE.

of the original microstructure. The multi-fiber domain is then tessellated into a network of Voronoi cells as shown in Fig. 4(a). The boundary of the RVE, shown in bold lines, is generated as the aggregate of the outside edges of Voronoi cells associated with the primary fibers (dark colored). The consequent SERVE (Fig. 4(b)) will have non-straight line edges corresponding to non-uniform fiber arrangements. However, nodes on the RVE boundary, created by this procedure are periodic, i.e. for every boundary node a periodic pair can be identified on the boundary at a distance of one period along one or both of the coordinate directions. In Fig. 4(a), the node pairs are identified as AA, BB etc. The periodicity constraint conditions on nodal displacements can then be easily imposed.

3.2. Adaptive mesh enrichment for level-0 and level-1 elements

Discretization error in level-0/1 elements is a result of insufficient orders of interpolation in the finite element model. The *hp*-adaptive mesh refinement suggested in [17] is adopted in this paper to

reduce the discretization error. The steps involved in this process are as follows:

- Evaluate the energy norm of the local error ϕ_k for element k, by solving the residual in the principal of virtual work as

$$\int_{\Omega^k_{l0/l1}} \Sigma_{ij}(\phi_k)e_{ij}(\mathbf{v})\,\mathrm{d}\Omega = \int_{\Omega^k_{l0/l1}} f_i v_i\,\mathrm{d}\Omega - \int_{\Omega^k_{l0/l1}} \Sigma_{ij}(\mathbf{u}_{l0/l1})e_{ij}(\mathbf{v})\,\mathrm{d}\Omega + \int_{\Gamma^k} (g_k)_i v_i\,\mathrm{d}\Gamma, \tag{8}$$

  where $(g_k)_i$ is the traction discontinuity on the element boundary Γ^k, $\Omega^k_{l0/l1}$ is the level-0/1 element boundary for element k and $\mathbf{u}_{l0/l1}$ is the solution obtained using the current polynomial p.
- Identify elements for *hp*-adaptivity from the condition $\phi_k \geqslant C_1(\phi_k)_{\max}$, where $(\phi_k)_{\max}$ is the maximum elemental local error. If an element is a candidate for adaptation, an exponent m is evaluated to determine the type of adaptivity i.e. if $p+2 \leqslant m$
  - then p refinement
  - else h refinement

  is performed. The singularity indicator m can be obtained by solving

$$\|\phi\|^2_k = \|\phi_{p+q}\|^2_k + C^2_k(p+q)^{-2(m-1)} \tag{9}$$

  for three different values of q as outlined in [17].

3.3. Transition elements between level-0/1 and level-2 elements

The interface between the macroscopic displacement based level-0 or level-1 elements, and level-2 elements requires a layer of transition elements for creating a smooth transition of variables as shown in Fig. 1. These elements (tr) are essentially level-2 elements with a displacement constraint imposed at the interface with level-0/1 elements. A direct constraint conforming with the displacement interpolation may however lead to spurious stresses. To avert these spurious stresses, a special interfacial layer is introduced between the transition elements and the level-0/level-1 elements. As suggested in [18], Lagrange multipliers are used to satisfy the interfacial displacement continuity constraint in a weak sense. The total potential energy of the multi-level element mesh may be expressed as

$$\Pi = \Pi_{\Omega_{l0}} + \Pi_{\Omega_{l1}} + \Pi_{\Omega_{l2}} + \Pi_{\Omega_{\mathrm{tr}}} + \int_{\Gamma_{\mathrm{int}}} \lambda_i^{l0/l1}(v_i - u_i^{l0/l1})\,\mathrm{d}\Gamma + \int_{\Gamma_{\mathrm{int}}} \lambda_i^{\mathrm{tr}}(v_i - u_i^{\mathrm{tr}})\,\mathrm{d}\Gamma, \tag{10}$$

where $\Pi_{\Omega_{l0}}$, $\Pi_{\Omega_{l1}}$, $\Pi_{\Omega_{l2}}$ and $\Pi_{\Omega_{\mathrm{tr}}}$ are the total potential energies for elements in level-0 (Ω_{l0}), level-1 (Ω_{l1}), level-2 (Ω_{l2}) subdomains and transition (Ω_{tr}) regions, respectively. Γ_{int} corresponds to the interfacial layer. $\lambda^{l0/l1}$ and λ^{tr} are Lagrange multipliers on Γ_{int}, corresponding to boundaries of $\Omega_{l0/l1}$ and Ω_{tr}, respectively. The interfacial displacements on the boundaries of $\Omega_{l0/l1}$ and Ω_{tr} elements at the interface are designated as $\mathbf{u}^{l0/l1}$ and $\mathbf{u}^{\mathrm{tr}}$. Derivation of the matrix forms of stiffness and force vectors for the model with various levels is discussed in detail in [15,16].

4. Numerical example of a double lap composite joint without damage

Adhesive bonded joints are optimal methods of joining structural components, because of their light weight due to the absence of fasteners. These joints are increasingly being used to repair damaged

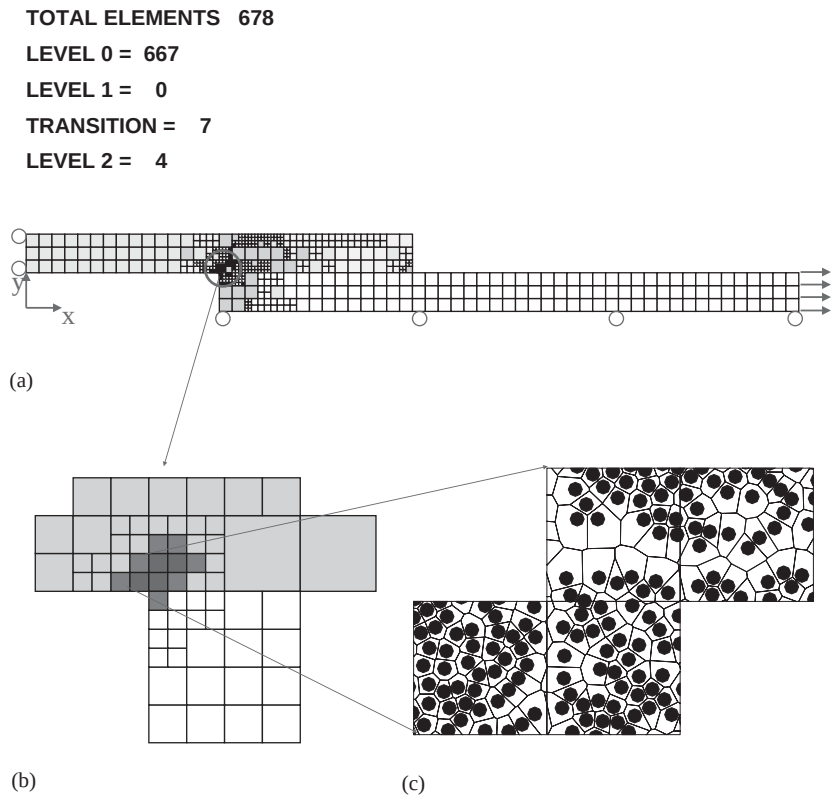

Fig. 5. (a) Macroscopic model of the multi-level mesh showing boundary conditions; (b) zoomed in region of the macroscopic mesh undergoing level transition; (c) microscopic analysis in the level-2 regions with VCFEM.

metallic structures in aircraft industries [19]. However, adhesively bonded structures consisting of two different materials, can induce high stresses near the interface leading to failure initiation by fiber cracking, fiber–matrix interfacial debonding or interfacial delamination. With this quest, a double-lap bonded joint with aluminum and boron–epoxy composite as the adherents is analyzed in this example. The joint is shown in Fig. 2. The dimension h is assumed to be 64 mm which corresponds to a total of 14 million fibers in the composite laminate. A perfect interface is assumed between the aluminum and the composite materials and the adhesive is not modeled explicitly. Only a quarter of the joint is modeled from considerations of symmetry in boundary and loading conditions. Symmetry boundary conditions are employed with displacement component u_y set to zero along the face $y=0$ and u_x displacement to zero along the face $x=0$, with coordinate axes depicted in Fig. 5(a). A unit displacement u_x is applied at the face $x=h$. The material properties of aluminum are: Young's modulus, $E=73.8$ GPa and Poisson's ratio, $v=0.25$. The composite material, at the microstructural level, consists of epoxy matrix with Young's modulus, $E=3.45$ GPa and Poisson's ratio, $v=0.35$, and boron fiber with Young's modulus, $E=413$ GPa and Poisson's ratio, $v=0.2$. The microstructure in this problem corresponds to that discussed in Section 3.1 and the representative material element, consisting of 18 fibers, is used for effective property evaluation. The components of the effective

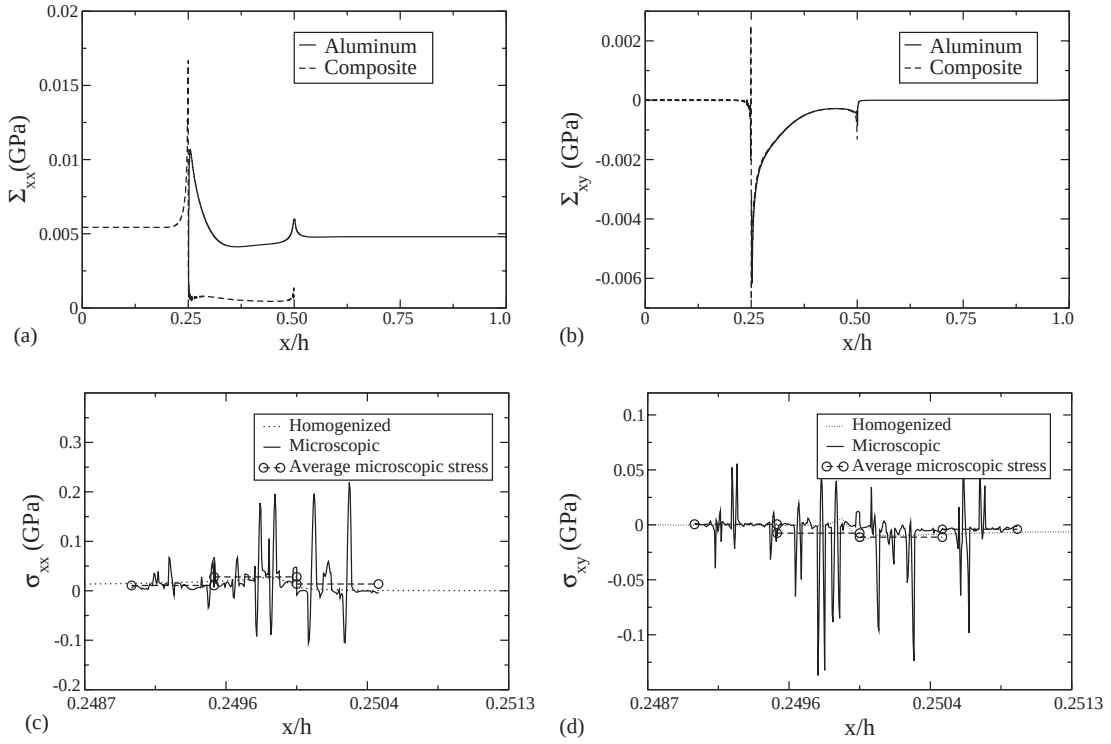

Fig. 6. Distribution of macroscopic stresses (a) Σ_{xx}; (b) Σ_{xy} in aluminum and composite material at $y/h = 0.05$ with the homogenized model, distribution of macroscopic, microscopic and averaged microscopic stresses; (c) σ_{xx}; (d) σ_{xy} at $y/h = 0.05$ near the point A.

elastic stiffness matrix (in GPa) are: $E_{1111} = 9.93$, $E_{1122} = 4.39$, $E_{1133} = 4.14$, $E_{2222} = 10.59$, $E_{2233} = 4.27$, $E_{1212} = 2.58$, $E_{3333} = 137.32$. The initial level-0 mesh consists of 225 level-0 QUAD4 elements. The level-0 *hp*-adaptation is performed following the procedure explained in Section 3.2.

The results of a pure macroscopic analysis are shown in Fig. 6. Stresses Σ_{xx} and Σ_{xy} at the bonded interface $y = 0.05h$ are plotted in this figure as a function of the x co-ordinate. In the composite, a high gradient of tensile stress Σ_{xx} results near the interface A at $x/h = 0.25$, with a high peak at A. Subsequently, Σ_{xx} drops to a very small value from $x/h = 0.25$ to 0.5. The composite stress Σ_{yy} is compressive and exhibits a singular behavior near the interface A at $x/h = 0.25$, due to material mismatch and free-edge constraints. The compressive nature of the stress inhibits delamination with macroscopic damage laws in this region. The shear stress Σ_{xy} is generally zero in the composite along this line, with the exception near A. In this region, it also exhibits a sharp gradient with a reversal in sign. The small peaks at $x/h = 0.5$ result from the composite free-edge conditions. In the aluminum panel, the stresses Σ_{xx} and Σ_{xy} start from zero at $x/h = 0.25$ and reach a maximum with a very high gradient near the point A. Subsequently, they stabilize at lower values, satisfying the traction free boundary conditions on the top surface $y/h = 0.05$. The stress Σ_{yy} stress is also compressive and very high near the interface $x/h = 0.25$. These macroscopic results match the predictions of stresses in bonded joints made in [19] in a qualitative sense.

Returning to the multi-scale analysis, the adapted multiple levels showing the microstructural region are depicted in Fig. 5. The level-0 to level-1 transition follows the criteria

$$E_k \left(\frac{(\Sigma_{\text{eqv}})_k}{(\Sigma_{\text{eqv}})_{\max}} \right) \geqslant C_1 E_{\text{avg}}, \tag{11}$$

where $(\Sigma_{\text{eqv}})_k$ is a measure of the equivalent stress in the element k. The constant C_1 is chosen with an understanding of the problem in question and error in element k, E_k is evaluated as

$$E_k^2 = \frac{\int_{\partial\Omega^k_{\text{hom}}} [[\Sigma_{xx}]]^2 \, \mathrm{d}\partial\Omega}{\int_{\partial\Omega^k_{\text{hom}}} \mathrm{d}\partial\Omega}. \tag{12}$$

Here Σ_{xx} is the dominant macroscopic stress component.

Physical criteria are used to determine locations of level-2 regions. A measure of the departure from periodicity conditions in the microstructural RVE may be taken as an indicator for this transition. For example, invoke the change if

$$\frac{\hat{\mathbf{F}}(\sigma_{ij}, \varepsilon_{ij})^{l1} - \hat{\mathbf{F}}(\sigma_{ij}, \varepsilon_{ij})^{\text{RVE}}}{\hat{\mathbf{F}}(\sigma_{ij}, \varepsilon_{ij})^{\text{RVE}}} \geqslant C_2, \tag{13}$$

where the function $\hat{\mathbf{F}}$ provides a measure of a quantity of interest in terms of local variables $(\sigma_{ij}, \varepsilon_{ij})$ that are deemed important. For example, in this problem $\hat{\mathbf{F}}$ is expressed as the average inclusion σ_{xx} stress in the microstructure. The superscript $l1$ corresponds to evaluating the function for the entire microstructure contained in each level-1 element by solving a local boundary value problem with level-0 macroscopic displacement solutions imposed on level-1 element boundary. The superscript RVE on the other hand corresponds to evaluation of the function within each RVE by imposing macroscopic strains with periodic boundary conditions on the RVE.

The parameters $C1$ and $C2$ are taken to be 0.1 and 0.3, respectively. The evolved multi-level mesh in Fig. 5 has 667 level-0 elements, 7 transition elements and 4 level-2 elements, which were previously level-1 elements. The level-2 elements consist of a total of 203 microstructural Voronoi cell elements. Fig. 6(c,d) compares: (a) the macroscopic stress using the homogenized model (level-0), (b) the microscopic stress obtained from level-2 VCFEM analysis, and (c) the average of the microscopic, along the x-direction near the critical point A. It is interesting to note that the homogenized stresses do not match with the average microscopic stresses near A. However, they are the same away from the critical region, proving that homogenization is, at least, not effective at critical singular regions.

5. The VCFEM for microstructures with interfacial debonding

Micromechanics problems of elastic–plastic composites and porous media with evolving damage by particle cracking using VCFEM have been solved in Ghosh and Moorthy [7,12], while elastic composites with interfacial debonding induced damage have been analyzed in Ghosh et al. [8,11]. In the latter work, the VCFEM is coupled with cohesive zone models to depict interfacial debonding as a phenomenon of progressive separation across a cohesive zone that is resisted by cohesive

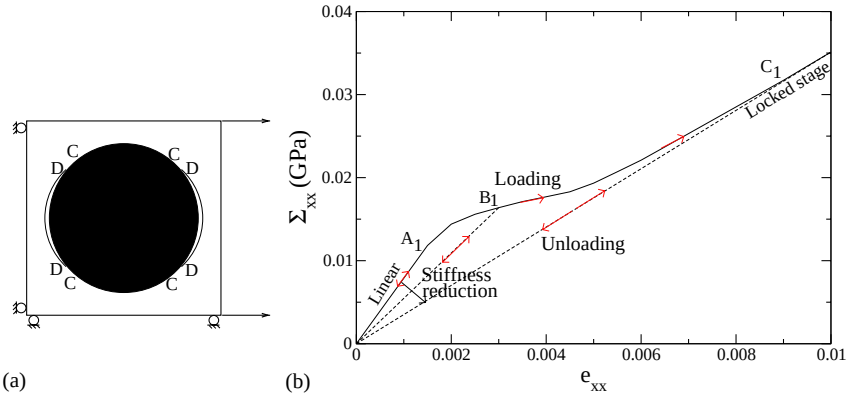

Fig. 7. (a) RVE subjected to loading in simple tension represented by a single Voronoi cell element; (b) Macroscopic stress–strain curve.

tractions. A bilinear cohesive zone model, postulated by Ortiz and Pandolfi [20], is used in this work to represent interfacial debonding. In this model, the traction at the interface increases linearly to a maximum value of $\sigma_{\max}$ corresponding to a displacement jump of δ_c before it starts decreasing to zero at a value of δ_e. In the softening region ($\delta_c < \delta < \delta_e$), the unloading proceeds along a linear path from the current position to the origin with a reduced stiffness. When the normal displacement is negative, stiff penalty springs with high stiffnesses are introduced between the node-pairs at the interface. Failure initiation and propagation due to interfacial debonding has been studied in detail for complex microstructures with arbitrary shapes and sizes by Ghosh et al. [8,11].

The VCFEM model is used to understand the effect of progressively increasing debonding on the macroscopic behavior of the composite. The RVE considered is a square domain with a single circular fiber with a volume fraction of 20%. The matrix material has Young's modulus, $E_{\mathrm{m}} = 4.6$ GPa and Poisson's ratio, $v_{\mathrm{m}} = 0.4$, while the fiber material has a Young's modulus $E_{\mathrm{f}} = 210$ GPa and Poisson's ratio, $v_{\mathrm{f}} = 0.3$. The cohesive law parameters for the interface are $\sigma_m = 0.02$ GPa, $\delta_c = 5.0 \times 10^{-5}$ m and $\delta_e = 20 \times 10^{-4}$ m. Fig. 7(a) shows the macroscopic or averaged stress–strain curve along the loading direction corresponding to simple tension loading. Three distinct regions emerge in this figure with increased loading. They are: (a) linear region from 0 till A_1 corresponding to the hardening domain in the interface with displacement jump $\delta \leqslant \delta_c$; (b) a non-linear region from A_1 to C_1 corresponding to softening and subsequent debonding with displacement jump $\delta > \delta_c$; and (c) a linear region beyond C_1 indicating that no further softening or debonding can take place for any additional external loading. Unloading from any point in the non-linear stage results in a linear stress –strain behavior with no residual stress or strain at O, as shown by the line $B_1 - O$. Reloading causes the stress–strain behavior to follow the path $O - B_1 - C_1$. Unloading from beyond C_1 follows a linear path to the origin. As seen in Fig. 7(a), the debonding is symmetric about the mid-plane and the top and bottom of the interface are in states of compression (C–C in Fig. 7(a)). This prevents further debonding of the interface leading to a constant post-debonding macroscopic stiffness. This exercise lays the foundation for a robust continuum damage mechanics model that is developed in this work from detailed micromechanical analyses.

6. A fourth-order continuum damage mechanics model from VCFEM-based micromechanical analysis

In CDM, macroscopic constitutive models involving macroscopic internal variables are used to represent material behavior with evolving micro-defects or micro-damage. The set of internal variables typically chosen are scalar, second order tensor or fourth order tensor leading to the so-called scalar isotropic, orthotropic and anisotropic damage models.

The general form of CDM models [21,22] introduce a fictitious effective stress $\tilde{\Sigma}_{ij}$ acting on an effective resisting area ($\tilde{A}$), which is caused by reduction of the original resisting area A due to material degradation caused by the presence of microcracks and stress concentration in the vicinity of cracks. The effective stress is related to the actual Cauchy stress Σ_{ij} in the damaged material using the fourth order damage effect tensor M_{ijkl} as

$$\tilde{\Sigma}_{ij} = M_{ijkl}(D_{ijkl})\Sigma_{kl}, \tag{14}$$

where D_{ijkl} is the damage tensor, can be of zeroth, second or fourth order, depending on the model employed. The hypotheses based on equivalence of elastic energy proposed by Cordebois and Sidoroff [23] is then used to establish a relation between the damaged and undamaged stiffnesses. In this hypothesis, the elastic energy for a damaged material with the actual stress is assumed to be equivalent in form to that of the undamaged material with the fictitious effective stress. This principle has been used in the damage modeling of Chow and Wang [24], Zhu and Cescotto [25], Voyiadjis et al. [26] and others and will be pursued in this work. The equivalence is established by equating the elastic energy in the damaged state to that in a hypothetical undamaged state as

$$W(\Sigma, D) = \frac{1}{2}\,\Sigma_{ij}(E_{ijkl}(D))^{-1}\Sigma_{kl} = W(\tilde{\Sigma}, 0) = \frac{1}{2}\,\tilde{\Sigma}_{ij}(E^0_{ijkl})^{-1}\tilde{\Sigma}_{kl}. \tag{15}$$

Here E^0_{ijkl} is the initial undamaged stiffness and $E_{ijkl}(D)$ is the stiffness of the damaged material. Substituting Eq. (14) into Eq. (15), the relation between the damaged and undamaged stiffnesses is established as

$$E_{ijkl} = (M_{pqij})^{-1}E^0_{pqrs}(M_{rskl})^{-1}. \tag{16}$$

With an appropriate choice of the order of the damage tensor and the assumption of a function for M_{ijkl}, Eq. (16) can be used to evaluate a damage model using micromechanics and homogenization. Through a series of examples it has been demonstrated in [27] that due to the different behavior of the cohesive zone in tension and compression, for an RVE with initial orthotropic macroscopic stiffness becomes completely anisotropic especially in tension/shear coupled loading conditions. Consequently, continuum damage model using scalar and second order damage tensor capable of exhibiting atmost an orthotropic behavior [28] cannot be used to model this type of material behavior.

6.1. Anisotropic damage model with fourth-order damage tensor

Anisotropic damage models involving fourth-order damage variables are able to overcome shortcomings of the scalar and second-order damage models. Such models have been proposed by e.g. Ortiz [29] for concrete in which loading surface is defined in stress space and the secant compliance tensor is considered as an internal variable. Simo and Ju [9] have proposed a loading surface in the

strain space with the current damaged stiffness tensor as an internal variable. Anisotropic damage in this work is introduced through positive projection strain tensors. The proposed model in this paper extends the Simo–Ju strain based damage model to account the anisotropic evolution of stiffness degradation. The damage surface in this model is expressed in terms of the strain e_{ij} and the damage work W_d as

$$F = \frac{1}{2} e_{ij} P_{ijkl} e_{kl} - \kappa(\alpha W_d) = 0, \tag{17}$$

where P_{ijkl} symmetric negative definite fourth order tensor that should be determined, α is a scaling parameter accounting for non-uniform damage work, κ is a parameter that is a function of the damage work $W_d = \int \frac{1}{2} e_{ij} \mathrm{d}E_{ijkl} e_{kl}$. It is important to introduce the scaling parameter α in conjunction with the damage work to account for its variability with the loading path, as explained in [27]. From the definition of the rate of damage work $\dot{W}_d$, $\frac{1}{2} e_{ij} e_{kl}$ is the conjugate to $\dot{E}_{ijkl}$. Using the associativity rule, the rate of stiffness degradation can be obtained as

$$\dot{E}_{ijkl} = \dot{\lambda} \frac{\partial F}{\partial(1/2 e_{ij} e_{kl})} = \dot{\lambda} P_{ijkl}. \tag{18}$$

It may be inferred from this Eq. (18) that P_{ijkl} corresponds to the direction of the rate of stiffness degradation tensor $\dot{E}_{ijkl}$. The model necessitates the evaluation of $\kappa(W_d)$, α and P_{ijkl}, which can be accomplished by micromechanical RVE analyses with periodicity boundary conditions. Determination of these parameters is discussed next.

6.2. Determination of $\kappa(W_d)$ and $\alpha(e_{ij})$

Evaluation of the function $\kappa(W_d)$ involves calculating this function for a reference loading path (strain combination) and scaling it for all other load paths with respect to this reference. In this paper, the reference loading path is chosen to be ($e_{xx} \neq 0$, all other $e_{ij} = 0$). Micromechanical simulation of the RVE is performed for this load path with periodic boundary conditions. The corresponding damage surface Eq. (17) for this loading becomes

$$\frac{1}{2} e_{xx}^2 P_{1111} - \kappa = 0. \tag{19}$$

Without loss of generality, the value of P_{1111} may be set to 1 and thus $\kappa = \frac{1}{2} e_{xx}^2$. The values of W_d can be evaluated numerically at the end of each increment. The functional form of $\kappa(W_d)$ is shown in Fig. 8. In the undamaged range, κ increases slightly for no damage work W_d. On the other hand, it asymptotically reaches increasing value at the damage saturation value corresponding to W_d^F, since κ keeps increasing even without any increase in W_d. Once the maximum value W_d^F is determined for the reference loading condition, α for any strain path can be obtained by simple scaling as

$$\alpha(e_{xx}, e_{yy}, e_{xy}) = \frac{W_d(e_{xx}, e_{yy}, e_{xy})}{W_d(e_{xx} \neq 0, e_{yy} = 0, e_{xy} = 0)}. \tag{20}$$

6.3. Determination of $P_{ijkl}(e)$

The damage parameters P_{ijkl} have been assumed to be constant in the Neilsen and Schreyer model described in Carol et al. [28]. However, for composite material with interfacial debonding,

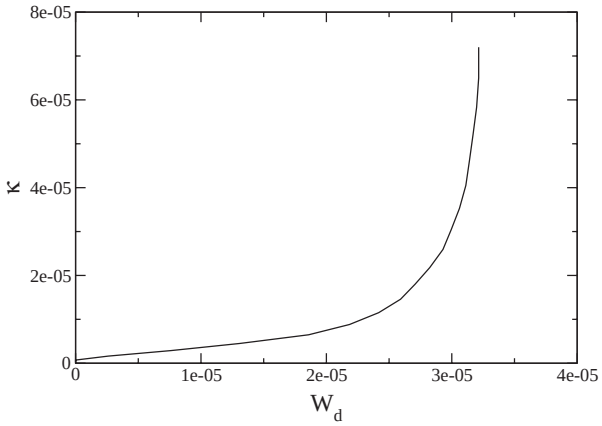

Fig. 8. Plot of κ vs. W_d for an RVE loaded along the macroscopic strain path $e_{xx} \neq 0$, $e_{yy} = e_{xy} = 0$.

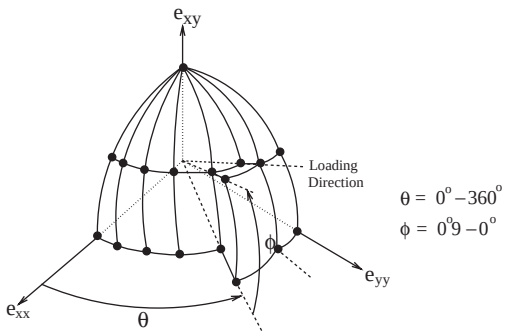

Fig. 9. Discretized macroscopic strain space for P_{ijkl} evaluation where the strain increments are prescribed as $\Delta e_{xx} : \Delta e_{yy} : \Delta e_{xy} = \cos\theta\cos\phi : \sin\theta\cos\phi : \sin\phi$.

the direction of rate of stiffness degradation varies significantly with increasing damage as shown in [27]. Consequently, components of $P_{ijkl}(e_{mn})$ are considered to be functions of the total strain and damage work, but their dependence on load history is assumed to be negligible in this work.

Due to the lack of a comprehensive functional form of $P_{ijkl}(e_{mn})$, a discrete approach, similar to that used in FEM is adopted in this paper. Discrete values of P_{ijkl} are evaluated at points in the macroscopic strain space by homogenization of the RVE based micromechanics analyses at systematic intervals along various strain paths. In the discretized strain space of Fig. 9, the value of a piecewise continuous P_{ijkl} at any point in the strain space may then be obtained by interpolation from nodal values according to

$$P_{ijkl}(e_{xx}, e_{yy}, e_{xy}) = \sum_{\alpha=1}^{8} (P_{ijkl})_\alpha N_\alpha(e_{xx}, e_{yy}, e_{xy}), \tag{21}$$

where $(P_{ijkl})_\alpha$ are the nodal values and N_α are the shape functions for a 3D linear 8-noded hexahedral element. A similar process has been discussed for porous elasto-plasticity in Ghosh et al. [4].

The nodal values of macroscopic stresses, the corresponding damage work W_d and P_{ijkl} are evaluated at each nodal point in a subspace of the e_{xx}–e_{yy}–e_{xy} space by solving incremental microscopic boundary value problems with VCFEM and asymptotic homogenization. In this process, macroscopic strain increments are applied to the RVE subjected to periodic boundary conditions. Strain increments are applied along the radial line in the macroscopic strain space such that a constant ratio is maintained between the strain components, i.e. $\Delta e_{xx} : \Delta e_{yy} : \Delta e_{xy} = \cos\theta\cos\phi : \sin\theta\cos\phi : \sin\phi$, where the angles θ and ϕ are depicted in Fig. 9. From the symmetry conditions, only half of the e_{xx}–e_{yy}–e_{xy} strain space is considered for loading, such that $0^0 \leqslant \theta \leqslant 360^0$ in the e_{xx}–e_{yy} plane and $0^0 \leqslant \phi \leqslant 90^0$ outside of this plane. The microscopic shear behavior is identical about the e_{xx} –e_{yy} plane except for the sign with and hence only the positive part is retained in ϕ range. The θ range encompasses the entire e_{xx}–e_{yy} plane, since the microscopic debonding behavior in tension and compression are different. The analyses are performed at uniform strain intervals of $\Delta\theta = 10°$, $\Delta\phi = 15°$. The P_{ijkl} evaluation algorithm is detailed in [27].

7. Numerical example of unit cell with debonding using CDM

The macroscopic finite element model with its constitutive relations represented by the CDM model is validated by comparison of results with those obtained by homogenizing VCFEM solutions in the RVE. The macroscopic model consists of a single QUAD4 element. For the microstructure, a square domain with a circular fiber of volume fraction 20% (see Fig. 10(a)) is considered. The material properties of the elastic matrix are $E_m = 4.6$ GPa, $\nu_m = 0.4$ and the elastic fiber are $E_m = 210$ GPa, $\nu_m = 0.3$. The interface properties are $\delta_c = 5.0 \times 10^{-5}$ m, $\delta_e = 20 \times 10^{-4}$ m and $\sigma_m = 0.02$ GPa. Five different macroscopic strain paths are considered for loading conditions, viz.

$$L1 : e_{xx} \neq 0, e_{yy} = e_{xy} = 0, \quad \text{(reference loading)}$$

$$L2 : e_{xx} = e_{yy} \neq 0, e_{xy} = 0,$$

$$L3 : e_{xy} \neq 0, e_{xx} = e_{yy} = 0,$$

$$L4 : e_{xx} = -e_{yy} \neq 0, e_{xy} = 0,$$

$$L5 : e_{xx} = e_{yy} = -e_{xy} \neq 0.$$

Periodicity conditions are enforced on the boundaries. The parameter $\kappa(W_d)$ is evaluated from the reference loading $(L1)$ corresponding to uniaxial tension. The strain states $(L2)$ and $(L3)$ correspond to biaxial and shear loading conditions respectively, while a combined tension–compression condition is represented by the load $(L4)$. Finally, the load $(L5)$ represents a combination of all strain components.

The macroscopic stress–strain plots with the CDM model are compared with the homogenized micromechanical (HMM) analyses in Fig. 10(b–f). All the nonzero stress components are plotted for each of the 5 loading conditions and excellent agreement is observed. For the biaxial loading, the interface fails completely at a strain of 0.0025. After this, the material exhibits a constant stiffness corresponding to an RVE with a void. In the shear loaded case, while Σ_{xx} and Σ_{yy} are zero prior to the onset of damage, they continue to increase with softening and debonding of the interface. This

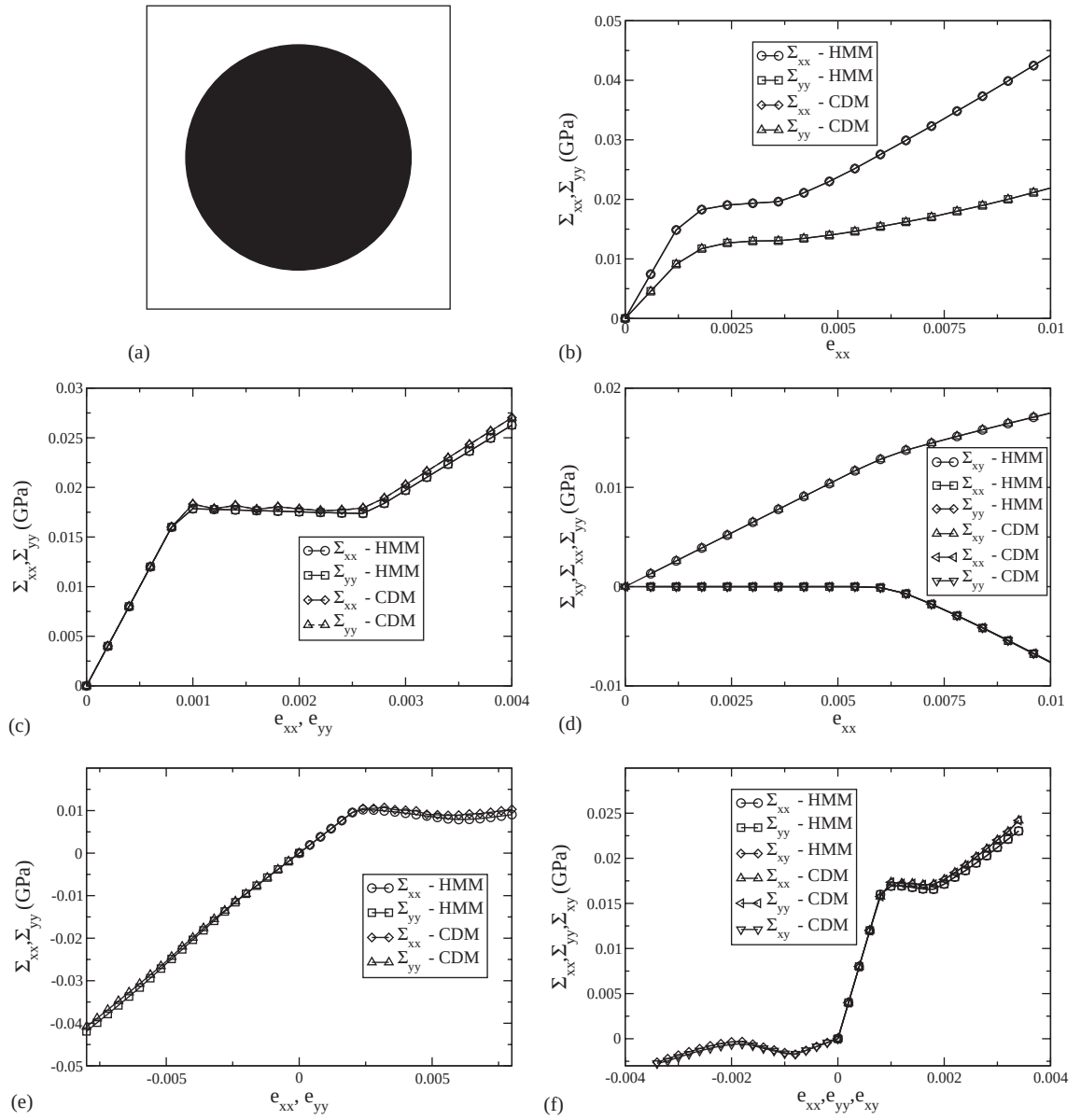

Fig. 10. Comparison of macroscopic stress–strain curves by continuum damage model and homogenized micromechanics for a (a) RVE with circular fiber for load cases; (b) $L1$; (c) $L2$; (d) $L3$; (e) $L4$; (f) $L5$.

is due to the different interface behavior in tension and compression. For the tension–compression case ($L4$), the behavior is almost linear in compression, whereas the macroscopic stresses in tension are significantly lower due to damage. For the combined straining case, a more complex stress–strain behavior is observed.

8. Numerical example of a double lap composite joint with damage

To demonstrate the effectiveness of the continuum damage model over the two scale analysis with asymptotic homogenization for a large structural problem, the aluminum composite joint discussed in Section 4 is considered. However, in this case, the RVE in the composite layer is assumed to undergo microstructural damage by interfacial debonding. The material properties of Aluminum are Youngs modulus, $E = 73.8$ GPa and Poisson's ratio, $v = 0.25$. The material properties of the composite are $E_{\mathrm{m}} = 4.6$ GPa and $v_{\mathrm{m}} = 0.4$ for the matrix and $E_{\mathrm{f}} = 210$ GPa and $v_{\mathrm{f}} = 0.3$ for the fibers, respectively. The RVE for the composite layer is assumed to contain a single fiber in a square domain with a volume fraction of 20% as shown in Fig. 10(a). The interface properties are $\sigma_m = 0.02$ GPa, $\delta_c = 5 \times 10^{-5}$ m and $\delta_e = 20 \times 10^{-4}$ m. A total uniform displacement of $u = 25 \times 10^{-4}$ h is applied over 20 equal increments. The uniform mesh contains 225 elements. Comparison of the results are made through macroscopic stress strain ($\Sigma_{xx} - e_{xx}$) curves at different locations in the structure as shown in Fig. 11. At locations A (Fig. 11(b)) and C (Fig. 11(d)), where the stress gradients are negligible, it can be observed that the difference between the CDM and HMM solutions are also negligible. However, near location B (Fig. 11(c)), the stress field is singular. The difference between the CDM and HMM is maximum at this region and is around 3.5%. Contour plots of macroscopic Σ_{xx} by the two approaches are also provided in Fig. 12 showing excellent agreement. Contour plot of macroscopic damage in Fig. 13(a) shows that regions in the composite layer to the left of point B are damaged due to a tensile state of stress. The region to the right of point B is in a state of compression and consequently there is no damage. Fig. 13(b) shows the microscopic stress and debonding for the RVE near point A. Although the results obtained by the two approaches are similar, the computational efficiency of the macroscopic analysis with the continuum constitutive model is far superior than the two scale analysis. For this particular problem, the time required for performing the analysis using continuum damage model is 70 s as compared to 142,200 s using two scale analysis. The scale up in efficiency for this problem is in the order of 2000 times and is therefore very desirable where only macroscopic results are of interest.

9. Conclusions

This paper presents an adaptive multi-level computational model that combines a conventional displacement based finite element model with a microstructural Voronoi cell finite element model for multi-scale analysis of composite materials. The model is developed with the capability to analyze both macroscopic and microscopic stresses and strains in real composite structures with non-uniform microstructural heterogeneities as obtained from optical or scanning electron micrographs. Three levels of hierarchy, with different resolutions, are introduced in this model to overcome shortcomings posed by modeling and discretization errors. Among the three levels are: (a) level-0, where pure macroscopic analysis is conducted using effective properties obtained by homogenization of variables in a statistical equivalent RVE; (b) level-1, which are intermediate regions of macro–micro coupled modeling, used for signaling the switchover from macroscopic analyses to pure microscopic analyses; and (c) level-2 regions of pure microscopic modeling where critical events in the microstructure are expected to occur. The adaptive Voronoi cell finite element model is utilized effectively for analysis of extended microstructural regions with high efficiency and accuracy. Special transition elements

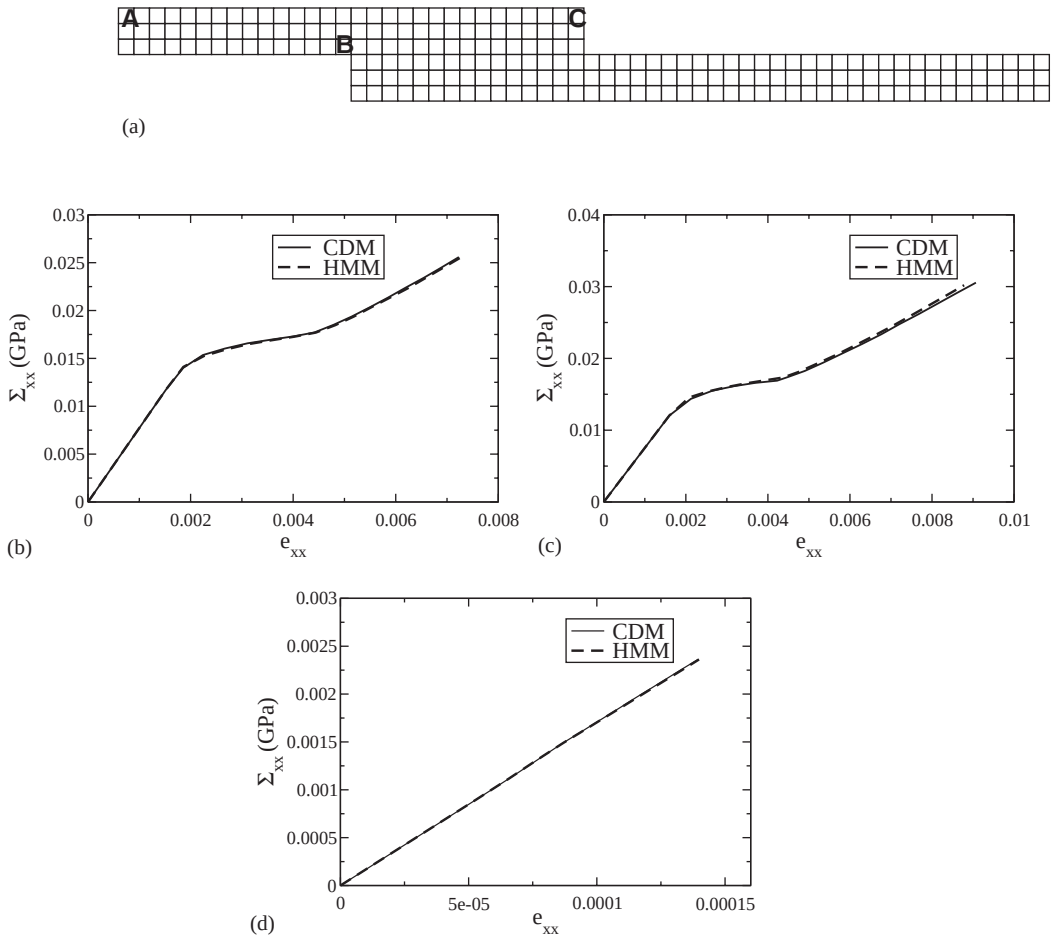

Fig. 11. (a) Mesh used for bonded joint case for comparing solution by CDM and HMM, Macroscopic stress–strain curve comparison for different locations in the structure; (b) at location A; (c) at location B; (d) at location C.

between level-0/1 and level-2 elements provide the necessary constraint conditions to facilitate smooth transition from macroscopic to microscopic analysis.

A robust macroscopic CDM model is developed for unidirectional fiber reinforced composites with interfacial debonding. The development of anisotropic damage model involves micromechanical analysis of the RVE using the VCFEM with subsequent homogenization. Parameters in the CDM model, describing the anisotropic stiffness degradation, vary significantly with evolving damage and microstructural variables. Specifically, a method for constructing damage-work dependent, piecewise continuous, anisotropic damage parameters is proposed by utilizing incremental loading paths and discrete data in the strain space. Numerical examples are conducted with this CDM for RVE under a wide variety of loading paths, represented by various strain combinations. Simultaneously micromechanical analyses of the RVE-based problems are executed using VCFEM for subsequent homogenization. The comparison between CDM and homogenized micromechanics results show

Fig. 12. Comparison of macroscopic Σ_{xx} (in GPa) contours by (a) continuum damage model and; (b) homogenized micromechanics.

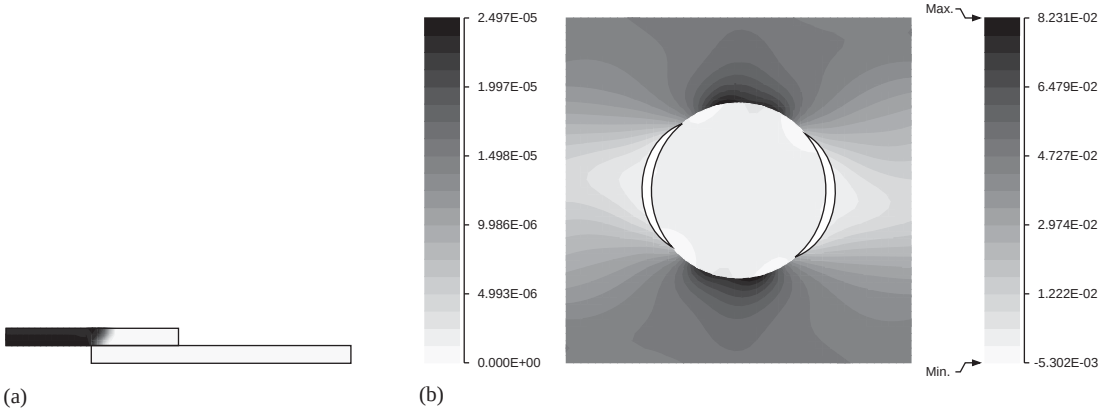

Fig. 13. (a) Contour plot of macroscopic damage by continuum damage model; (b) Microscopic σ_{xx} stress (in GPa) with debonding for the macroscopic element close to point A.

excellent agreement. Numerical example of an aluminum composite bonded joint demonstrate the computational efficiency gained by this effective CDM model when compared with the performance of two-scale damage models using asymptotic homogenization like [30,31].

However, the model proposed is restricted by the assumptions of the existence of an RVE in the presence of micro-damage. Effectively this means that it assumes uniformity of macroscopic variables as well as microscopic periodicity. Bulsara et al. [32] have studied methods of RVE size determination for non-uniform distribution with damage. Lacy et al. [33] have proposed higher order internal state variables based on the gradients of mesoscale damage distribution for RVE containing

distributed micro-cracks. It is well known that catastrophic failure occurs by the localization of damage, resulting in severe gradients. The two scale model will not be applicable in these regions because of its local nature. These regions would need the models to transcend scales to capture the localized damage growth as done in the elastic case of this paper as well as in the works of Ghosh et al. [4]. A true multi-scale model with interfacial debonding in conjunction with the CDM model is the subject of a future paper.

Acknowledgements

This work has been supported by the Air Force Office of Scientific Research through grant No. F49620-01-1-0305 (Program Director: Dr. B. L. Lee). This sponsorship is gratefully acknowledged. Computer support by the Ohio Supercomputer Center through grant # PAS813-2 is also gratefully acknowledged.

References

[1] A. Benssousan, J.L. Lions, G. Papanicoulau, Asymptotic Analysis for Periodic Structures, North-Holland, Amsterdam, 1978.
[2] N.J. Pagano, E.F. Rybicki, On the significance of effective modulus solutions for fibrous composites, J. Compos. Mater. 8 (1974) 214–228.
[3] J. Fish, K. Shek, Multiscale analysis of composite materials and structures, Comput. Sci. Tech. 60 (2000) 2547–2556.
[4] S. Ghosh, K. Lee, P. Raghavan, A multi-level computational model for multi-scale damage analysis in composite and porous materials, Int. J. Solids Struct. 38 (14) (2001) 2335–2385.
[5] J.T. Oden, T.I. Zohdi, Analysis and adaptive modeling of highly heterogeneous elastic structures, Comput. Meth. Appl. Mech. Eng. 148 (1997) 367–391.
[6] P. Raghavan, S. Moorthy, S. Ghosh, M.J. Pagano, Revisiting the composite laminate problem with an adaptive multi-level computational model, Comput. Sci. Tech. 61 (2001) 1017–1040.
[7] S. Moorthy, S. Ghosh, Adaptivity and convergence in the Voronoi cell finite element model for analyzing heterogeneous materials, Comp. Meth. Appl. Mech. Eng. 185 (2000) 37–74.
[8] S. Ghosh, Y. Ling, B. Majumdar, R. Kim, Interfacial debonding analysis in multiple fiber reinforced composites, Mech. Mater. 32 (2000) 561–591.
[9] J.C. Simo, J.W. Ju, Strain and stress-based continuum damage models, Part I: Formulation, Int. J. Solids Struct. 23 (7) (1987) 821–840.
[10] E. Sanchez-Palencia, Non-homogeneous media and vibration theory, Lecture notes in Physics 127, Springer-Verlag, Berlin, Heidelberg, 1980.
[11] S. Li, S. Ghosh, Influence of the local morphology to interfaces in multiple fiber reinforced composites, under review.
[12] S. Moorthy, S. Ghosh, A model for analysis of arbitrary composite and porous microstructures with Voronoi cell finite elements, Int. J. Numer. Meth. Eng. 39 (1996) 2363–2398.
[13] R. Pyrz, Correlation of microstructure variability and local stress field in two-phase materials, Mat. Sci. Eng. A 177 (1994) 253–259.
[14] S. Ghosh, Z. Nowak, K. Lee, Quantitative characterization and modeling of composite microstructures by Voronoi cells, Acta Mat. 45 (1997) 2215–2234.
[15] P. Raghavan, S. Ghosh, Adaptive multi-scale computational modeling of composite materials, Comput. Mod. Engg. Sci. 5 (2) (2004) 151–170.
[16] P. Raghavan, S. Ghosh, Concurrent multi-scale analysis of elastic composites by a multi-level computational model, Comput. Meth. Appl. Mech. Eng., under review.

[17] M. Ainsworth, B. Senior, Aspects of adaptive *hp*-finite element method: Adaptive strategy, conforming approximation and efficient solvers, Comput. Meth. Appl. Mech. Eng. 150 (1997) 65–87.
[18] M.A. Aminpour, J.B. Ransom, S.L. McCleary, A coupled analysis method for structures with independently modeled finite element subdomains, Int. J. Num. Meth. Eng. 38 (1995) 3695–3718.
[19] N. Rastogi, Som R. Soni, A. Nagar, Thermal stresses in aluminum-to-composite double-lap bonded joints, Adv. Eng. Software 29 (1998) 273–281.
[20] M. Ortiz, A. Pandolfi, Finite-deformation irreversible cohesive element for three-dimensional crack-propagation analysis, Int. J. Numer. Meth. Eng. 44 (1999) 1267–1282.
[21] L.M. Kachanov, Introduction to Continuum Damage Mechanics, M. Nijhoff, Dordrecht, Boston, 1987.
[22] J. Lemaitre, J.L. Chaboche, Mechanics of Solids, Cambridge University Press, Cambridge, 1990.
[23] J.P. Cordebois, F. Sidoroff, Anisotropic damage in elasticity and plasticity, J. Mec. Theor. Appl. (1982) 45–60.
[24] C.L. Chow, J. Wang, An anisotropic theory of elasticity for continuum damage mechanics, Int. J. Frac. 20 (1987) 381–390.
[25] Y.Y. Zhu, S. Cescotto, A fully coupled elasto-visco-plastic damage theory for anisotropic materials, Int. J. Solids Struct. 32 (11) (1995) 1607–1641.
[26] G.Z. Voyiadjis, P.I. Kattan, Advances in Damage Mechanics: Metals and Metal Matrix Composites, Elsevier, 1999.
[27] P. Raghavan, S. Ghosh, A continuum damage mechanics model for unidirectional composites undergoing interfacial debonding, Mech. Mat., under review.
[28] I. Carol, E. Rizzi, K. Willam, A unified theory of elastic degradation and damage based on a loading surface, Int. J. Solids Struct. 31 (20) (1994) 2835–2865.
[29] M. Ortiz, A constitutive theory for the inelastic behavior of concrete, Mech. Mater. 4 (1985) 67–93.
[30] J. Fish, Q. Yu, K. Shek, Computational damage mechanics for composite materials based on mathematical homogenization, Int. J. Numer. Meth. Eng. 45 (1999) 1657–1679.
[31] F. Lene, D. Leguillon, Homogenized constitutive law for a partially cohesive composite material, Int. J. Solids Struct. 18 (5) (1982) 443–458.
[32] V.N. Bulsara, R. Talreja, J. Qu, Damage initiation under transverse loading of unidirectional composites with arbitrarily distributed fibers, Composites Sci. Tech. 59 (1999) 673–682.
[33] T.E. Lacy, D.L. McDowell, R. Talreja, Gradient concepts for evolution of damage, Mechanics of Materials 31 (1999) 831–860.